ISSN 1063-7710, Acoustical Physics, 2011, Vol. 57, No. 2, pp. 230–240. © Pleiades Publishing, Ltd., 2011.
Original Russian Text © E.V. Glushkov, N.V. Glushkova, S.I. Fomenko, 2011, published in Akusticheskii Zhurnal, 2011, Vol. 57, No. 2, pp. 243–245.

WAVE PROCESSES IN THE MEDIA WITH MICRO- AND NANOSTRUCTURES

Influence of Porosity on Characteristics of Rayleigh-Type Waves in Multilayered Half-Space

E. V. Glushkov, N. V. Glushkova, and S. I. Fomenko
Kuban State University, ul. Stavropolskaya 149, Krasnodar, 350040 Russia
e-mail: evg@math.kubsu.ru
Received March 19, 2010

Abstract—Poroelastic fluid-saturated multilayered half-space is considered; particle motion in this half-space is described by Biot–Frenkel equations for two-phase media. A brief description of the derivation of integral and asymptotic representations for wave fields excited by a given surface load is presented; the influence of the porous microstructure on the form of dispersion curves and amplitude characteristics of excited traveling waves is analyzed. It is demonstrated using numerical examples that the amplitude of additional modes occurring due to the presence of a microstructure can be essentially larger than the amplitudes of principal modes present in the waveguide with purely elastic layers.

DOI: 10.1134/S1063771011020059

INTRODUCTION

Elastic porous media saturated by a fluid or a gas are an example of materials with microstructure. The necessity of investigation of wave processes in such media is due to applied problems of soil mechanics, geophysics, and vibroseismic exploration; the construction and oil and gas industries; and the occurrence of new granular–powder and sponge materials used, for example, for thermal and vibroinsulation of aerospace elements. At present, the commonly accepted tool for theoretical study of propagation of linear waves in porous fluid-saturated media is the Biot–Frenkel equations [1, 2] generalizing the equations of the classical theory of elasticity to the case of two-phase media. The motion of each of the phases (elastic skeleton and pore fluid) is described by the set of equations containing additional terms that take into account phase interaction. It is known that taking in to account the mutual influence of oscillations of particles of the elastic skeleton and pore fluid results in the change of the velocity of longitudinal (P_1) and transverse (S) body waves and the occurrence of the additional longitudinal wave (P_2) (a so-called slow longitudinal wave or Biot wave). It is difficult to excite and register the slow wave P_2; this is the reason why this wave was experimentally discovered 20 years after its theoretical prediction [3, 4]. On the whole, Biot's theory yields results that agree well with experimental measurements for velocities of body waves and their frequency dependences.

Microstructure is manifested in wave effects connected with the presence of boundaries. First, the laws (coefficients) of refraction and reflection of body waves incident on the interface of two-phase media change [5], and, second, not only characteristics of surface and channel waves propagating along straight boundaries change, but their number does not change: in the presence of porosity, additional traveling waves occur [6, 7]. Detailed analysis of the properties of waves occurring in the poroelastic half-space with a free boundary and at the interface of the poroelastic and fluid half-spaces can be found in [8–10]. This analysis is forestalled by the presentation of Biot's theory and detailed survey of studies in this field. In particular, it is pointed out that experimentally determined characteristics of interface waves [11] agree well with those obtained in the framework of Biot's theory [6] and the permeability coefficient K_r essentially influences these characteristics [12].

These theoretical studies as a rule are performed using the methods of modal analysis; in the framework of these methods the problem for the considered porous waveguide with homogeneous boundary conditions is reduced to the homogeneous algebraic system with respect to unknown coefficients of the general solution. The determinant of the matrix A of this system yields the dispersion equation for the sought traveling waves,

$$\Delta(\zeta, \omega) \equiv \det A(\zeta, \omega) = 0, \qquad (1)$$

and the displacement of the medium particle at passage of these waves is expressed in terms of the eigenvectors $\mathbf{t}_n$: $A(\zeta_n)\mathbf{t}_n = 0$ corresponding to real or close to real roots $\zeta = \zeta_n(\omega)$ of this equation. However, the eigenvectors $\mathbf{t}_n$ are determined to constant factors; therefore, in the framework of the modal analysis it is impossible to obtain the real ratio between the amplitudes of different modes excited by the given source.

For solution of the problem of excitation of the harmonic wave field $\mathbf{u}e^{-i\omega t}$ by the given source $\mathbf{q}e^{-i\omega t}$ in the waveguide with plane-parallel boundaries (half-space, layer, multilayered half-space or packet of layers) the method of integral Fourier transform with respect to horizontal coordinates F_{xy} is usually used; this method provides the solution in the form of the inverse Fourier integral of the product of Fourier symbols of the Green's matrix K of the medium and the given load vector $\mathbf{Q} = F_{xy}[\mathbf{q}]$ [13],

$$\mathbf{u}(\mathbf{x}) = F_{xy}^{-1}[K\mathbf{Q}]$$

$$\equiv \frac{1}{2\pi}\int_{\Gamma_1}\int_{\Gamma_2} K(\alpha_1,\alpha_2,z)\mathbf{Q}(\alpha_1,\alpha_2)e^{-i(\alpha_1 x+\alpha_2 y)}d\alpha_1 d\alpha_2, \quad (2)$$

$$\mathbf{x} = (x,y,z).$$

The integration contours Γ_1, Γ_2 go along the real axis and deviate from it to the complex plane to bypass the real poles ζ_n of elements of the matrix K. The residuals in these poles describe the surface and channel waves,

$$\mathbf{u}_n(\mathbf{x}) \sim \mathbf{a}_n(\varphi,z)e^{i\zeta_n r}/\sqrt{r}, \quad r/l \gg 1, \quad (3)$$

where l is the characteristic wavelength; r,φ are the polar radius and angle; and $x = r\cos\varphi$, $y = r\sin\varphi$. Waves (3) determined by the poles ζ_n include surface Rayleigh waves and channel Lamb, Stoneley, Scholte, and Love waves; below, they will be called Rayleigh-type or Rayleigh waves for brevity.

The poles ζ_n coincide with the roots of dispersion equation (1) derived in the framework of the modal analysis and the amplitude factors $\mathbf{a}_n$ are proportional to displacements described by the corresponding eigen-solutions. However, unlike the latter, they are unambiguously expressed in terms of the residuals $\operatorname{res} K|_{\alpha=\zeta_n}$, $\alpha = \sqrt{\alpha_1^2+\alpha_2^2}$ and the values of $\mathbf{Q}$ for $\alpha_1 = -\zeta_n\cos\varphi, \alpha_2 = -\zeta_n\sin\varphi$ (see, e.g., [14, 15] and references therein for details of derivation of (2), (3)). Thus, the amplitude of each mode (3) is strictly defined, which makes it possible to calculate the dynamic reaction of the medium and the amount of wave energy received from the given source (load $\mathbf{q}$) and analyze its distribution between excited modes using integral representation (2).

The method of derivation of integral and asymptotic representations (2) and (3) (i.e., methods of construction of the matrix K, determination of real and close to the real axis poles ζ_n and their residuals) is quite well developed not only for multilayered isotropic elastic media [16, 17], but also for more complex structures, such as, for example, stratified media with gradient dependence of elastic properties on the depth z [16] or arbitrarily anisotropic layered waveguides [18]. It is natural to try to use a similar approach to the case of poroelastic materials try to find out whether the amplitude of additional surface and channel waves determined by the microstructure (porosity) can be, unlike P_2, comparable with the amplitude of principal Rayleigh-type waves. It was indicated in [19] that the history of construction of wave fields from a point source in a porous Biot medium began in late 1970s–early 1980s [20, 21], but is mainly limited by cases of homogeneous infinite space or half-space [22]. In spite of papers concerning multilayered poroelastic media with sources published in the recent years, results on the influence of porous microstructure on the amplitude of Rayleigh-type waves are very few. Note that traveling waves occur due to the porosity on plane-parallel and cylindrical fluid-saturated well waveguides. Numerical analysis of amplitudes of waves excited in such a structure by a point source of expansion–compression was performed in [23].

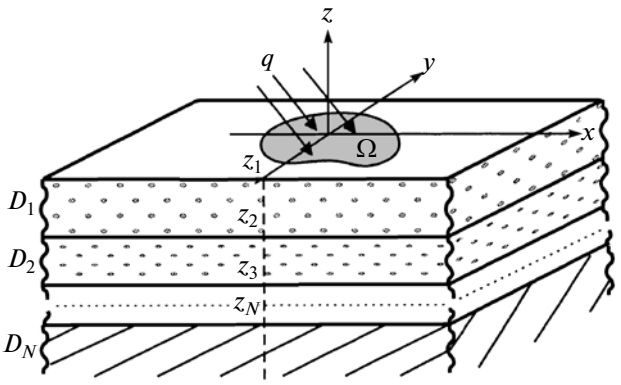

Fig. 1. Multilayered poroelastic half-space with surface load.

STATEMENT OF THE PROBLEM

The N-layered half-space $D: -\infty < x,y < \infty$, $-\infty < z \le 0$, consisting of $N-1$ layers D_k: $z_{k+1} \le z \le z_k$ with the finite thickness $h_k = z_k - z_{k+1}$ and the lower half-space D_N: $-\infty < z \le z_N$ is considered (Fig. 1). It is assumed that the layer material can be two-phase poroelastic (Biot medium) and purely elastic, i.e., without a microstructure. In the latter case the porosity coefficient $\varepsilon = V^f/V$ characterizing the volume fraction of the fluid phase V^f in some volume of the porous material V is equal to zero. Layers are ideally connected with each other, i.e., the conditions of continuity of displacements $\mathbf{u} = (u_x,u_y,u_z)^T = (u_1,u_2,u_3)^T$ and stresses $\boldsymbol{\tau} = (\tau_{xy},\tau_{yz},\sigma_z)^T = (\tau_1,\tau_2,\tau_3)^T$ are satisfied at the internal boundaries $z = z_k$, $k = 2,\ldots,N$, and in the case of contact of two porous materials these conditions are added by the conditions of continuity of pore pressure p^f and the normal component $\dot{w}_3$ of

the relative velocity vector $\dot{\mathbf{w}} = \varepsilon(\dot{\mathbf{u}}^s - \dot{\mathbf{u}}^f)$ (for definiteness the boundaries are assumed permeable with free flow of the pore fluid). Correspondingly, the upper surface $z = z_1 = 0$ is free from stresses ($\boldsymbol{\tau} = 0$) and the pore fluid pressure ($p^f = 0$, pores are open) beyond the region of application of the surface load $\mathbf{q}$.

According to the Biot's theory, averaged over the elementary volume displacements of the porous material $\mathbf{u}$ are the sum of displacements of the elastic skeleton $\mathbf{u}^s$ and the pore fluid $\mathbf{u}^f$,

$$\mathbf{u} = (1-\varepsilon)\mathbf{u}^s + \varepsilon\mathbf{u}^f$$

(hereinafter, the indices s and f denote the quantities related to the elastic and fluid phases of the material, respectively). Similarly, σ_{ij}^s and σ_{ij}^f denote the averaged components of the stress tensor $\sigma_{ij} = \sigma_{ij}^s + \sigma_{ij}^f$ connected with the deformation ε_{ij} by the generalized Hooke's law [2],

$$\begin{aligned} \sigma_{ij}^s &= \lambda e^s \delta_{ij} + 2\mu\varepsilon_{ij}^s + Qe^f\delta_{ij}, \\ \sigma^f &= \frac{1}{3}\sigma_{ii}^f = -\varepsilon p^f = Qe^s + Re^f, \\ \varepsilon_{ij}^\nu &= (u_{i,j}^\nu + u_{j,i}^\nu)/2, \quad i,j = 1,2,3. \end{aligned} \tag{4}$$

Here, $e^\nu = \varepsilon_{ii}^\nu = \operatorname{div}\mathbf{u}^\nu$ is the volume expansion, $\nu = s$ or f, δ_{ij} is the Kronecker symbol. As usually, in the case of indexed notation summing over the repeated indices is assumed, and the indices after the comma denote the derivative with respect to the corresponding coordinate x_j: $\mathbf{x} = (x,y,z) = (x_1,x_2,x_3)$. The constants λ, μ, R, Q are the macroscopic elastic moduli of the porous medium depending on the microstructure of the porous material. For $\varepsilon = 0$ the moduli λ, μ coincide with the Lame constants λ^s, μ^s for the material of the elastic skeleton, $Q = R = 0$, and first relation (4) degenerates into the Hooke's law for the isotropic linearly elastic medium.

The motion of elementary volume of the porous medium satisfies the equilibrium equations

$$\begin{aligned} \sigma_{ij,j}^s &= \rho_{11}\ddot{u}_i^s + \rho_{12}\ddot{u}_i^f + \gamma\dot{w}_i, \\ \sigma_{ij,j}^f &= \rho_{12}\ddot{u}_i^s + \rho_{22}\ddot{u}_i^f - \gamma\dot{w}_i, \; i = 1,2,3, \end{aligned} \tag{5}$$

after substituting relations (4) these equations yield the motion equations in terms of displacements,

$$\begin{aligned} &\nabla[(\lambda+2\mu)\operatorname{div}\mathbf{u}^s + Q\operatorname{div}\mathbf{u}^f] \\ &+ \mu\Delta\mathbf{u}^s - \rho_{11}\ddot{\mathbf{u}}^s - \rho_{12}\ddot{\mathbf{u}}^f - \gamma\dot{\mathbf{w}} = 0, \\ &\nabla[Q\operatorname{div}\mathbf{u}^s + R\operatorname{div}\mathbf{u}^f] - \rho_{12}\ddot{\mathbf{u}}^s - \rho_{22}\ddot{\mathbf{u}}^f + \gamma\dot{\mathbf{w}} = 0, \end{aligned} \tag{6}$$

the first of these equations for zero porosity ($\varepsilon = 0$) degenerates into the Lame equations for the elastic medium ($\mathbf{u} = \mathbf{u}^s$, $\rho = \rho^s$),

$$(\lambda+2\mu)\nabla\operatorname{div}\mathbf{u} + \mu\Delta\mathbf{u} - \rho\ddot{\mathbf{u}} = 0. \tag{7}$$

Here, $\rho_{11}, \rho_{12}, \rho_{22}$ are the inertia coefficients connected with the densities of the elastic and fluid phases ρ^s and ρ^f as

$$\begin{aligned} \rho_{11} &= (1-\varepsilon)\rho^s - \rho_{12}, \\ \rho_{22} &= \varepsilon\rho^f - \rho_{12}, \quad \rho_{12} = \varepsilon(1-\tilde{\alpha})\rho^f, \end{aligned} \tag{8}$$

and $\tilde{\alpha}$ is the pore tortuosity coefficient; the coefficient γ at $\dot{\mathbf{w}}$ determines the level of dissipation of the wave energy (analogue of the viscous medium). In the examples considered below the skeleton is assumed to be ideally elastic, and the pore fluid non-viscous, and as a consequence, $\gamma = 0$. Points above the variables denote time derivatives.

Below the problem is formulated for the case of established harmonic oscillations $\mathbf{u}e^{-i\omega t}$, i.e., it is formulated with respect to the frequency spectrum of the displacement vector connected with nonstationary oscillations by Fourier transform with respect to time F_t,

$$\begin{aligned} \mathbf{u}(\mathbf{x},\omega) &= F_t[\mathbf{u}(\mathbf{x},t)] = \int_0^\infty \mathbf{u}(\mathbf{x},t)e^{i\omega t}dt, \\ \mathbf{u}(\mathbf{x},t) &= F_t^{-1}[\mathbf{u}(\mathbf{x},\omega)] = \frac{1}{\pi}\operatorname{Re}\int_0^\infty \mathbf{u}(\mathbf{x},\omega)e^{-i\omega t}d\omega. \end{aligned} \tag{9}$$

In this case the time derivative in (5)–(7) is replaced by the factor $-i\omega$: $\dot{\mathbf{w}}(t) \to -i\omega\mathbf{w}(\omega)$, $\ddot{\mathbf{u}}(t) \to -\omega^2\mathbf{u}(\omega)$ and the nonstationary displacements are calculated if necessary by numerical integration over ω according to (9). The harmonic factor $e^{-i\omega t}$ is omitted below.

The representation of the stress vector $\boldsymbol{\tau}$ on the horizontal surface z =const with the normal $\mathbf{n} = (0,0,1)^T$ in terms of the displacement vector $\mathbf{u}$ necessary for formulation of boundary conditions has the form

$$\begin{aligned} \boldsymbol{\tau} = \boldsymbol{\tau}^s + \boldsymbol{\tau}^f, \quad \boldsymbol{\tau}^s &= (\lambda e^s + Qe^f)\mathbf{n} + 2\mu\mathbf{u}_{,3}^s + \mu(\mathbf{n}\times\operatorname{rot}\mathbf{u}^s), \\ \boldsymbol{\tau}^f &= (Qe^s + Re^f)\mathbf{n} = -\varepsilon p^f\mathbf{n}, \end{aligned}$$

or in terms of components,

$$\begin{aligned} \tau_i^s &= \mu\left(u_{3,i}^s - u_{i,3}^s\right), \quad \tau_i^f = 0, \quad i = 1,2, \\ \tau_3^s &= \lambda e^s + 2\mu u_{3,3}^s + Qe^f, \quad \tau_3^f = Qe^s + Re^f. \end{aligned}$$

In the case of the medium with open pores the boundary conditions on the upper surface $z = 0$ have the form

$$\boldsymbol{\tau}|_{z=0} = \begin{cases} \mathbf{q}(x,y), & (x,y) \in \Omega \\ 0, & (x,y) \notin \Omega, \end{cases}$$
$$\tau_3^f|_{z=0} = \begin{cases} \varepsilon q_3(x,y), & (x,y) \in \Omega \\ 0, & (x,y) \notin \Omega. \end{cases} \quad (10)$$

Here, $\mathbf{q} = (q_1, q_2, q_3)^T$ is the vector of arbitrary surface load applied to the domain Ω. Below numerical results for the medium with closed pores are presented for comparison. For this medium it is assumed that on the surface $z = 0$ free flow of the pore fluid is absent,

$$w_3|_{z=0} = 0 \quad \text{for} \quad \forall x, y. \quad (11)$$

In this case the condition for τ_3^f in (10) is replaced by condition (11).

The conditions on the permeable boundaries between the poroelastic layers D_{k-1} and D_k have the form

$$[\mathbf{u}]_k = 0, \quad [\boldsymbol{\tau}]_k = 0, \quad [w_3]_k = 0, \quad [p^f]_k = 0. \quad (12)$$

Hereinafter, square brackets denote the jump of a corresponding function of z at the interface $z = z_k$,

$$[\mathbf{u}]_k = \lim_{\delta \to 0} (\mathbf{u}|_{z_k - \delta} - \mathbf{u}|_{z_k + \delta}).$$

If one medium is purely elastic ($\varepsilon = 0$), the first three conditions of (12) remain unchanged (assuming that for $\varepsilon = 0$ $\mathbf{u} = \mathbf{u}^s$, $\boldsymbol{\tau} = \boldsymbol{\tau}^s$, $\mathbf{w} = 0$) and the fourth one is rejected (the pressure ρ^f at the interface with the elastic medium is not determined).

The condition of zero displacement at infinity closes the formulation of the boundary value problem,

$$\lim_{|\mathbf{x}| \to \infty} \mathbf{u} = 0, \quad z \le 0, \quad |\mathbf{x}| = \sqrt{x^2 + y^2 + z^2},$$

in the case of the ideal medium ($\gamma = 0$) this condition is added by the radiation condition following from the principle of limiting absorption: the homogeneous limit of the corresponding problem with absorption $\gamma > 0$ for $\gamma \to 0$ is taken as the problem solution for the ideal medium.

It is known that displacements of the elastic medium can be expressed in terms of the scalar and vector potentials φ and ψ: $\mathbf{u} = \nabla\varphi + \mathrm{rot}\,\boldsymbol{\psi}$, thus splitting Lame equations (7) into independent wave equations with respect to φ and $\boldsymbol{\psi}$. For porous medium, the similar representation contains two scalar potentials φ_1, φ_2. According to [2, 5], it is convenient to write this equation in the form

$$\mathbf{u}^s = \nabla\varphi_1 + m_2\nabla\varphi_2 + \mathrm{rot}\,\boldsymbol{\psi},$$
$$\mathbf{u}^f = m_1\nabla\varphi_1 + \nabla\varphi_2 + m_3\mathrm{rot}\,\boldsymbol{\psi}, \quad (13)$$

in which the constants m_k are chosen in such a way that, if (13) is substituted into Eqs. (6) transformed to the frequency representation, the latter are split into the independent scalar Helmholtz equations and the vector equation with respect to the vortex potential,

$$\Delta\varphi_j + \kappa_j^2\varphi_j = 0, \ \kappa_j = \omega/v_{pj}, j = 1,2,$$
$$\mathrm{rot}\,\mathrm{rot}\,\boldsymbol{\psi} + \kappa_s^2\boldsymbol{\psi} = 0, \ \kappa_s = \kappa_3 = \omega/v_s. \quad (14)$$

In this case v_{p1}, v_{p2}, and v_s are the velocities of body waves P_1, P_2, and S. Only two components of the vortex potential $\boldsymbol{\psi}$ are independent; therefore, without losing generality it can be written as $\boldsymbol{\psi} = \left(g'_y, -g'_x, \psi\right)^T$ which reduces the vector equation with respect to $\boldsymbol{\psi}$ to two scalar Helmholtz equations,

$$\Delta g + \kappa_3^2 g = 0, \quad \Delta\psi + \kappa_3^2\psi = 0. \quad (15)$$

The splitting is achieved if the vectors $\mathbf{m}_1 = (1, m_1)^T$ and $\mathbf{m}_2 = (m_2, 1)^T$ satisfy the homogeneous matrix equations

$$\left(C - \kappa_j^2 B\right)\mathbf{m}_j = 0, j = 1,2,$$
$$C = \begin{pmatrix} \lambda + 2\mu & Q \\ Q & R \end{pmatrix}, \quad B = \begin{pmatrix} \rho_{11} + i\gamma/\omega & \rho_{12} - i\gamma/\omega \\ \rho_{12} - i\gamma/\omega & \rho_{22} + i\gamma/\omega \end{pmatrix},$$

i.e., are the eigenvectors corresponding to the eigenvalues κ_j,

$$\det\left(C - \kappa_j^2 B\right) = 0,$$
$$\kappa_{1,2} = \frac{\omega^2}{2}\left[a \mp \sqrt{a^2 - 4\Delta_C\Delta_B}\right]/\Delta_C,$$
$$\Delta_C = \det C, \quad \Delta_B = \det B,$$
$$a = R\rho_{11} - 2Q\rho_{12} + (\lambda + 2\mu)\rho_{22} + i\gamma(\lambda + 2\mu + 2Q + R)/\omega. \quad (16)$$

In the case of independent phase motion ($Q = 0$, $\rho_{12} = 0$) they coincide with the wave numbers for longitudinal waves in the elastic skeleton ($\kappa_1 = \omega^2\rho_{11}/(\lambda + 2\mu)$) and pore fluid ($\kappa_2 = \omega^2\rho_{22}/R$). For S waves

$$\kappa_3^2 = \omega^2\left[\frac{(\rho_{11}\rho_{22} - \rho_{12})^2 + i(\rho_{11} + \rho_{22} + 2\rho_{12})\gamma/\omega}{\mu(\rho_{22} + i\gamma/\omega)}\right].$$

The constants m_j included in (13) have the form

$$m_1 = -\left[(\lambda + 2\mu)\kappa_1^2 - \omega^2\rho_{11} - i\gamma\omega\right]/\Delta,$$
$$m_2 = -\left[R\kappa_2^2 - \omega^2\rho_{22} - i\gamma\omega\right]/\Delta,$$
$$m_3 = (\omega\rho_{12} - i\gamma)/(\omega\rho_{22} + i\gamma),$$
$$\Delta = Q\kappa_2^2 - \omega^2\rho_{12} + i\gamma\omega.$$

GREEN'S MATRIX OF POROELASTIC HALF-SPACE

Columns of the Green's matrix $k(\mathbf{x}) = F_{xy}^{-1}[K]$ (see (2)) are the fundamental solutions of the considered problem corresponding to the concentrated surface loads $\tau|_{z=0} = \delta(x,y)\ \mathbf{i}_j$ applied along the coordinate unit vectors $\mathbf{i}_j, j = 1,2,3$. For the arbitrary load $\mathbf{q}$, the solution is written in the form of convolution of the Green's matrix k and $\mathbf{q}$,

$$\mathbf{u}(\mathbf{x}) = k*\mathbf{q} \equiv \int\int_{\Omega} k(x-\xi, y-\eta, z)\mathbf{q}(\xi,\eta)d\xi d\eta,$$

or in equivalent form (2) in terms of the product of their Fourier symbols K and $\mathbf{Q}$. According to the representation of $\mathbf{u}$ in terms of $\mathbf{u}^s$ and $\mathbf{u}^f$, the Green's matrix of the porous medium is composed of the matrices k^s and k^f for the averaged displacements of the skeleton and the fluid,

$$k = (1-\varepsilon)k^s + \varepsilon k^f,$$
$$\mathbf{u}^s = k^s * \mathbf{q}, \quad \mathbf{u}^f = k^f * \mathbf{q}.$$

The general method for derivation of the algorithm for calculation of elements of the matrix $K(\alpha_1, \alpha_2, z)$ is the application of the Fourier transform F_{xy} with respect to the horizontal coordinates x, y, which reduces the initial equations for each layer D_k to the system of linear ordinary differential equations with respect to z. The unknown constants included in the general solution to these systems united in the vector $\mathbf{t}$ are then determined from the systems of linear algebraic equations

$$A\mathbf{t} = \mathbf{f}_j, \quad \mathbf{f}_j = (\mathbf{i}_j, 0, \ldots, 0)^T, j = 1,2,3, \tag{17}$$

which occur for satisfaction of the transformed boundary conditions at the upper surface,

$$\mathbf{T}|_{z=0} = \mathbf{i}_j, \quad \mathbf{T} = F_{xy}[\boldsymbol{\tau}], \quad j = 1,2,3$$

and internal boundaries $z = z_k, k = 2,3,\ldots,N$.

In the case of the anisotropic medium when the explicit representation of the general solution is too cumbersome, the following approach proved to be good [18]: the Fourier transform is formally applied with respect to all three (rather than two) spatial variables $\mathbf{x}$: $\mathbf{U}(\boldsymbol{\alpha}) = F_{\mathbf{x}}[\mathbf{u}]$, $\boldsymbol{\alpha} = (\alpha_1, \alpha_2, \alpha_3)$. In this case the factors α_3 included in the obtained expressions are actually the symbolic notation of the operator of differentiation with respect to z: $\left(\frac{d}{dz}\right)^p \to (-i\alpha_3)^p$, $p = 1,2$. Thus, the compact matrix form of the transformed equations, their general solutions, and the algorithm of construction of the matrix K become possible.

In the considered case, this approach makes it possible to reduce Eqs. (6) for the ideal medium ($\gamma = 0$) to the homogeneous system with the dimension 6×6,

$$[B(\boldsymbol{\alpha}) - \omega^2 C]\mathbf{V}(\alpha_1, \alpha_2, z) = 0 \tag{18}$$

with respect to the vector $\mathbf{V} = (\mathbf{U}^s, \mathbf{U}^f)^T$, $\mathbf{U}^\nu = F_{xy}[\mathbf{u}^\nu]$, $\nu = s, f$. Here,

$$B = \begin{pmatrix} B^{(1)} & B^{(2)} \\ B^{(3)} & B^{(4)} \end{pmatrix}, \quad C = \begin{pmatrix} \rho_{11} I & \rho_{12} I \\ \rho_{12} I & \rho_{22} I \end{pmatrix},$$

I is the unit matrix 3×3, and $B^{(n)}$, $n = 1,\ldots,4$ are 3×3 blocks with the components

$$b_{ij}^{(1)} = (\lambda + 2\mu)\alpha_i\alpha_j + \mu\beta^2\delta_{ij},$$
$$b_{ij}^{(2)} = b_{ij}^{(3)} = Q\alpha_i\alpha_j, b_{ij}^{(4)} = R\alpha_i\alpha_j, \quad i,j = 1,2,3,$$
$$\beta^2 = |\boldsymbol{\alpha}|^2 = \alpha_1^2 + \alpha_2^2 + \alpha_3^2, \quad \alpha^2 = \alpha_1^2 + \alpha_2^2.$$

The general solution to system (18) has the form

$$\mathbf{V} = \sum_{n=1}^{8} t^{(n)}\mathbf{v}_n e^{\lambda_n z}, \tag{19}$$

where $t^{(n)}$ are the unknown coefficients, $\lambda_n = \lambda_n(\alpha_1, \alpha_2, \omega)$ are the roots of the characteristic equations with respect to the parameter α_3, and $\mathbf{v}_n$ are the corresponding eigenvectors,

$$\Delta(\boldsymbol{\alpha}, \omega) = \det[B(\boldsymbol{\alpha}) - \omega^2 C] = 0,$$
$$[B(\alpha_1, \alpha_2, \lambda_n) - \omega^2 C]\mathbf{v}_n = 0.$$

The number of terms in (19) is equal to eight, since $\Delta(\boldsymbol{\alpha}, \omega)$ is the eighth-order polynomial with respect to α_3.

In the anisotropic case, the roots λ_n and the eigenvectors are numerically determined from the similar equations, but in the considered case, due to the splitting of the original system into independent Helmholtz equations (14), (15) they can be written in the explicit form,

$$\lambda_j = \sigma_j, \lambda_4 = \lambda_3, \lambda_{n+4} = -\lambda_n,$$
$$\sigma_j = \sqrt{\alpha^2 - \kappa_j^2}, j = 1,2,3, n = 1,\ldots,4.$$

The roots $\pm\sigma_3$ are twofold, and for $\alpha \neq \kappa_3$ ($\sigma_3 \neq 0$) they correspond to two pairs of eigenvectors $\mathbf{v}_3, \mathbf{v}_4$ and $\mathbf{v}_7, \mathbf{v}_8$. For $\alpha = \kappa_j$ (at branch points) in the Jordan form of the matrix $B - \omega^2 C$ Jordan cells occur and the root $\sigma_j = 0$ corresponds to the eigenvectors and adjoint vectors. The form of general solution (19) should change correspondingly, but this case has no special practical value, since branch points are rounded by the integration contour and, which the most important, in the case of minimal variation of α, representation (19) is valid.

The form of the general solution to transformed equations (14), (15) is

$$\Phi_1(\alpha, z) = t^{(1)}e^{\sigma_1 z} + t^{(5)}e^{-\sigma_1 z},$$
$$\Phi_2(\alpha, z) = t^{(2)}e^{\sigma_2 z} + t^{(6)}e^{-\sigma_2 z},$$
$$G(\alpha, z) = t^{(3)}e^{\sigma_3 z} + t^{(7)}e^{-\sigma_3 z},$$
$$\Psi(\alpha, z) = t^{(4)}e^{\sigma_3 z} + t^{(8)}e^{-\sigma_3 z},$$

and that of relations between the Fourier symbols of the functions included in them which follows from (13) is

$$\mathbf{U}^s(\boldsymbol{\alpha}) = -i\boldsymbol{\alpha}(\Phi_1 + m_1\Phi_2) + \mathbf{r}(\boldsymbol{\alpha}),$$
$$\mathbf{U}^f(\boldsymbol{\alpha}) = -i\boldsymbol{\alpha}(m_1\Phi_1 + \Phi_2) + m_3\mathbf{r}(\boldsymbol{\alpha}),$$
$$\mathbf{r}(\boldsymbol{\alpha}) = F_x[\mathrm{rot}\,\boldsymbol{\psi}] = \mathbf{a}(\boldsymbol{\alpha})G + \mathbf{b}(\boldsymbol{\alpha})\Psi,$$
$$\mathbf{a} = (-\alpha_1\alpha_3, -\alpha_2\alpha_3, \alpha^2)^T, \quad \mathbf{b} = (-i\alpha_2, i\alpha_1, 0)^T,$$

these representations can be used to easily to obtain the explicit form of the eigenvectors $\mathbf{v}_n = \left(\mathbf{v}_n^s, \mathbf{v}_n^f\right)^T$,

$$\begin{aligned}
\mathbf{v}_{1,5} &= (-i\boldsymbol{\alpha}, -im_1\boldsymbol{\alpha})^T\,|_{\alpha_3=\pm i\sigma_1},\\
\mathbf{v}_{2,6} &= (-im_2\boldsymbol{\alpha}, -\boldsymbol{\alpha})^T\,|_{\alpha_3=\pm i\sigma_2},\\
\mathbf{v}_{3,7} &= (\mathbf{a}(\boldsymbol{\alpha}), m_3\mathbf{a}(\boldsymbol{\alpha}))^T\,|_{\alpha_3=\pm i\sigma_3},\\
\mathbf{v}_{4,8} &= (\mathbf{b}(\boldsymbol{\alpha}), m_3\mathbf{b}(\boldsymbol{\alpha}))^T\,|_{\alpha_3=\pm i\sigma_3},
\end{aligned} \tag{20}$$

for the first value of the index n in $\mathbf{v}_n$ the upper plus sign is taken in the substitution α_3, and for the second one, the lower minus sign.

Based on representations similar to (19), the general solution $\mathbf{V}_k(\alpha_1, \alpha_2, z)$ for each porous layer D_k can be written in the form of the product of the known matrix and the vector of unknown coefficients $\mathbf{t}_k = \left(t_k^{(1)}, t_k^{(2)}, \ldots, t_k^{(8)}\right)^T$,

$$\mathbf{V}_k = M_k E_k(z)\mathbf{t}_k. \tag{21}$$

The columns of 6×8 matrix M_k are the vectors $\mathbf{v}_n$ of form (20) in which the constants m_j and κ_j are determined for the parameters of the kth layer, the matrix $E_k = \mathrm{diag}(e_1, \ldots, e_8)$ consists of the exponentials

$$e_j = e^{\sigma_j(z-z_k)}, \quad e_{j+4} = e^{-\sigma_j(z-z_{k+1})},$$
$$e_4 = e_3, \quad e_8 = e_7, \quad j = 1,2,3,$$

the shift of the argument $z - z_k$ and $z - z_{k+1}$ in the powers provides the numerical stability of solution to system (17).

The vector of unknown coefficients of this system $\mathbf{t}$ consists of the vectors $\mathbf{t}_k$ for each layer, $\mathbf{t} = (\mathbf{t}_1, \mathbf{t}_2, \ldots, \mathbf{t}_N)^T$, and the block diagonal structure of the matrix A is determined by the matrix relations

$$S_1\mathbf{t}_1 = \mathbf{i}_j, \quad j = 1,2,3,$$
$$C_{k-1}\mathbf{t}_{k-1} - C_k\mathbf{t}_k = 0, \quad k = 2,3,\ldots,N,$$

which occur if representations (21) and similar matrix representations for the Fourier symbols of the stress vector $\mathbf{T}$ and relative velocity $W_3 = F_{xy}[w_3]$ are substituted into the boundary conditions at the surface $z = 0$ and internal boundaries $z = z_k$, $k = 2,3,\ldots,N$. The block structure of the matrix A looks similar to that in the previous algorithms of K construction for layered elastic media [17, 18] with obvious differences in block representations. The main difficulty is the violation of unification due to the possible absence of porosity ($\varepsilon = 0$) in some layers. For these layers $\mathbf{V} = \mathbf{U}^s$ is the vector of length 3, and in representation (19) $t^{(2)} = t^{(7)} = 0$, i.e., actually only six unknowns are left. Thus, the dimensions of the blocks S_1 and C_k are different for the numbers k corresponding to porous or purely elastic layers. Note also that in representation (19) for the lower half-space ($k = N$) the exponentials $e^{-\sigma_j z}$ violating the radiation conditions for $\alpha < \kappa_j$ and exponentially growing for $\alpha > \kappa_j$, $z \to -\infty$ for the lower half-space, i.e., it is necessary to assume that $t^{(n)} = 0, n = 5,\ldots,8$.

In the case of a large number of layers N, it is reasonable to use the sparseness of the matrix A and organize the solution to system (17) using the chain of numerically stable recurrent matrix relations that require inversion of matrix blocks of relatively low dimension.

After determination of $\mathbf{t}$, jth columns of the matrices K^s and K^f for $z \in D_k$ are calculated using representation (21) (the first three components $\mathbf{V}_k = (\mathbf{U}_k^s, \mathbf{U}_k^f)^T$ are included in K^s, and the last three in K^f).

It should be noted that the same as in the case of the isotropic elastic medium the problem of construction of the matrix K can be split into two independent problems (analogue of separation of the problem for torsional oscillation or SH waves). The detailed description of this algorithm based on the determination of unknown coefficients $t_k^{(n)}$ from two independent linear algebraic systems is given in [24].

ANALYSIS OF THE INFLUENCE OF POROSITY ON CHARACTERISTICS OF EXCITED WAVES

In the case of investigation of wave processes in porous fluid-saturated media, samples with fixed material parameters are usually studied. In theoretical

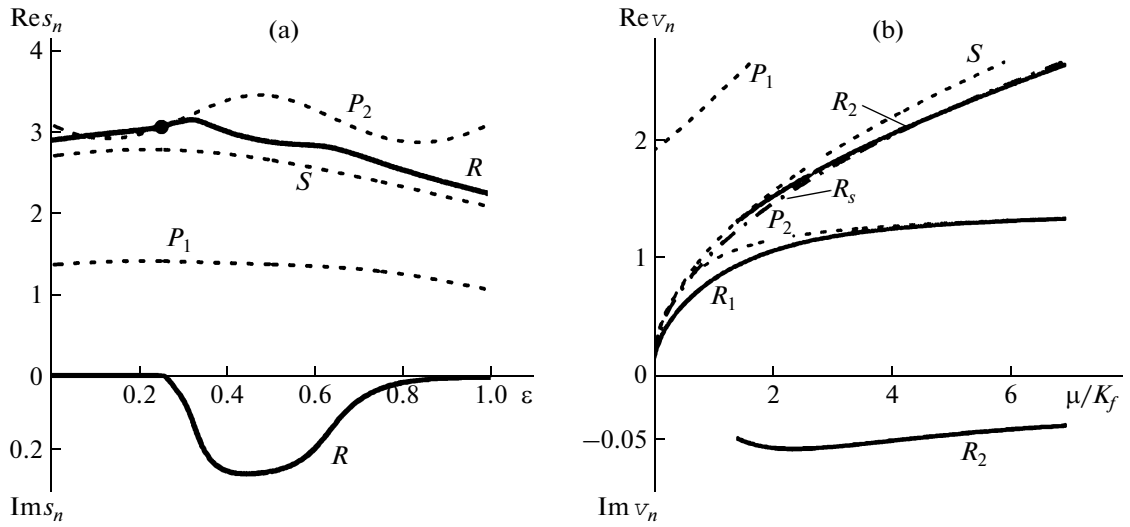

Fig. 2. (a) Slowness s_n of body and Rayleigh waves as a function of porosity ε; (b) phase velocity v_n as a function of the shear modulus μ for homogeneous porous half-space (comparison with [9, 25]).

simulation the parameters λ, R, Q included in motion equations (6) are calculated using the classical representations [2] in terms of the compression moduli K_s, K_f, and K_b for the material of elastic skeleton, pore fluid, and porous sample with dry pores which can be experimentally measured, as well as the shear modulus μ,

$$\lambda = K_b - \frac{2}{3}\mu + Q^2/R, \quad R = \varepsilon^2\Lambda_1, \quad Q = \varepsilon(\Lambda_0 - \varepsilon)\Lambda_1,$$
$$\Lambda_0 = 1 - K_b/K_s,$$
$$\Lambda_1 = K_s^2 K_f/[K_f(K_s - K_b) + \varepsilon K_s(K_s - K_f)].$$

Similarly, the inertia coefficients are expressed in terms of the experimentally determined densities ρ^s, ρ^f and the pore tortuosity $\tilde{\alpha}$ using relations (7).

The objective of this study is the investigation of the influence of porosity ε on the wave characteristics; for this purpose the input material parameters should be determined as functions of ε. Unfortunately, experimental determination of such dependences is hardly realized in practice; therefore, for numerical experiments the dependence of input parameters on ε is determined in such a way that for the intermediate value ε = 0.26 they coincide with the parameters of the medium used in [25] (for possible test representation of results) and in the limiting cases ε = 0 and 1 they approach the properties of the elastic and fluid phases,

$$\lambda(0) = \lambda^s, \quad \mu(0) = \mu^s, \quad \lambda(1) = \mu(1) = 0,$$
$$R(0) = 0, \quad R(1) = \lambda^f, \quad Q(0) = Q(1) = 0,$$
$$\rho_{12}(0) = \rho_{12}(1) = 0, \quad m_j(0) = m_j(1) = 0, \quad j = 1,2,3.$$

These requirements are satisfied, in particular, by the following dependences:

$$\lambda = \mu(\lambda^s - \lambda^f)/\mu^s + \lambda^f(1-\varepsilon) - Q,$$
$$\mu = \mu^s(1-\varepsilon)(1 + c_{\mu 1}\varepsilon + c_{\mu 2}\varepsilon^2),$$
$$R = \lambda^f\varepsilon(1 + c_R\varepsilon(1-\varepsilon)), \quad Q = \lambda^f\varepsilon^2(1-\varepsilon)^2 c_Q,$$
$$\rho_{12} = -c_\rho\varepsilon^2(1-\varepsilon)^2\rho^f, \tag{22}$$

The inertia coefficients ρ_{11}, ρ_{22} are determined by (8). The agreement with the parameters from [25] is achieved for the following values of the coefficients:

λ^s	μ^s	λ^f	ρ^s	ρ^f	c_ρ	$c_{\mu 1}$	$c_{\mu 2}$	c_Q	c_R
0.671	0.359	0.085	2600	820	0.0632	1750	21.357	−0.552	1.21

(23)

The elastic moduli λ and μ are determined in GPa (1 GPa = 10^9 n/m^2), the density ρ in kg/m^3, and the other coefficients are dimensionless.

Figure 2 shows the results for the homogeneous half-space ($N = 1$) with the same parameters as in [9, 25] for verification. The values of phase velocities $v_n = \omega/\zeta_n$ and inverse to them slowness factors $s_n = \zeta_n/\omega$ are compared; according to (3), they are determined in terms of the poles ζ_n of elements of the symbols of the Green's matrix K. In Fig. 2a solid lines

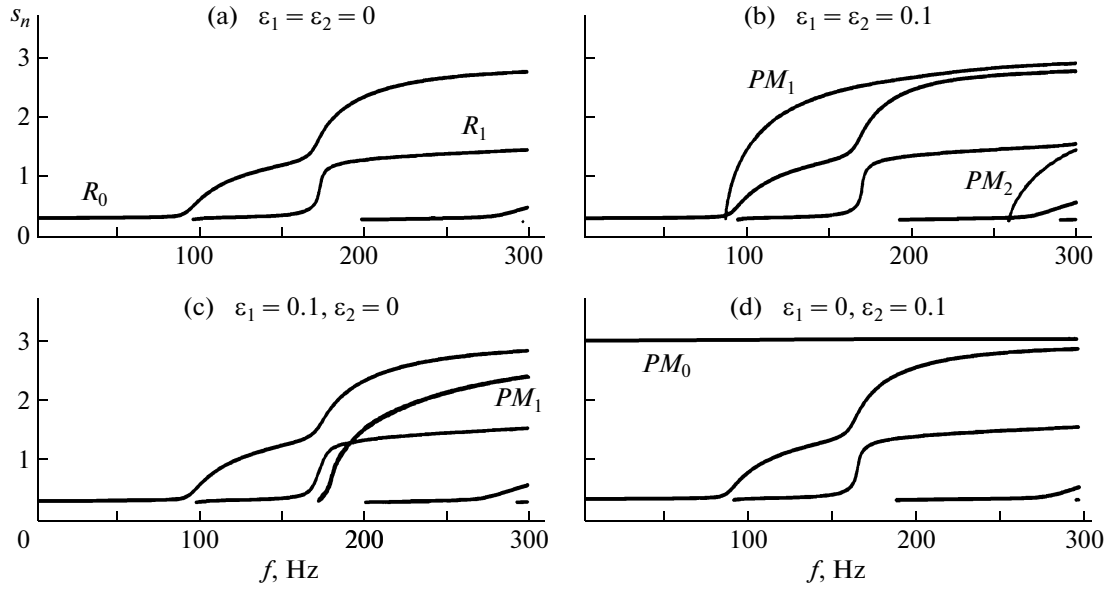

Fig. 3. Dispersion curves for the three-layered half-space for different combinations of porosity $\varepsilon_1, \varepsilon_2$ of two upper layers.

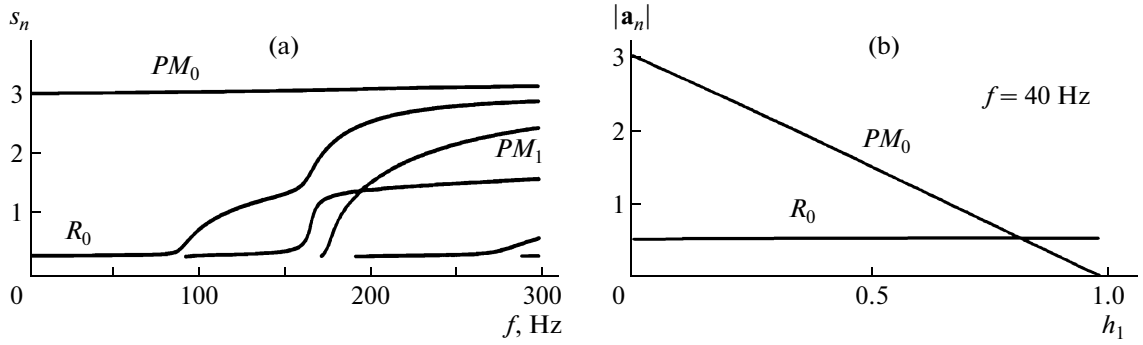

Fig. 4. (a) Dispersion curves for closed pores on the upper surface; (b) amplitudes of pore and Rayleigh modes as functions of the upper layer thickness.

show the dependences of ε on the real and imaginary parts of the slownesses s_R (in s/km) for Rayleigh-type waves (R) and dashed lines show the slownesses of body waves P_1, P_2, S calculated according to (14) and (16); the dark circle shows the value of s_R for $\varepsilon = 0.26$ taken from [25]. The Rayleigh pole $\zeta_R = \zeta_1$ and the corresponding slowness s_R are real only for those values of ε for which $s_R > s_{P_2}$, i.e., approximately in the range $0.05 < \varepsilon < 0.26$. In the range $0.26 < \varepsilon < 0.85$ the pole is rather far from the real axis and returns toward it without reaching it for $\varepsilon > 0.85$. In the case of complex ζ_R Rayleigh wave (3) propagates with exponential attenuation $e^{-|\mathrm{Im}\,\zeta_R|r}$ which becomes essential in the range $0.26 < \varepsilon < 0.85$, while for $\varepsilon < 0.05$ and $\varepsilon > 0.85$ the attenuation $\theta = \mathrm{Im}\,\zeta_R/\mathrm{Re}\,\zeta_R$ is very small ($\theta \approx 10^{-5}$).

The right-hand side of Fig. 2b shows the dependences of the phase velocities v_n on the ratio of the shear modulus μ and the pore fluid compression modulus K_f for the water-saturated half-space with the parameters $\varepsilon = 0.3$, $K_s = 360$ GPa, $K_f = 2.35$ GPa, $\rho^s = 2650$ kg/m^3, $\nu^p = 0.2$, and $\tilde{\alpha} = 1.25$ (ν^p is the Poisson coefficient of the porous medium without a pore fluid) considered in [9]. These curves for the velocities of body waves (P_1, P_2, S) and Rayleigh wave R_1 coincide with those shown in Fig. 6 from [9], but the latter figure does not contain the curve R_2 for the second Rayleigh-type wave. The pole ζ_2 determining this wave is complex with the imaginary part yielding the attenuation θ of order 10^{-2}. Since the characteristics of this wave are close to the slowness of the Rayleigh wave for the elastic half-space with the parameters

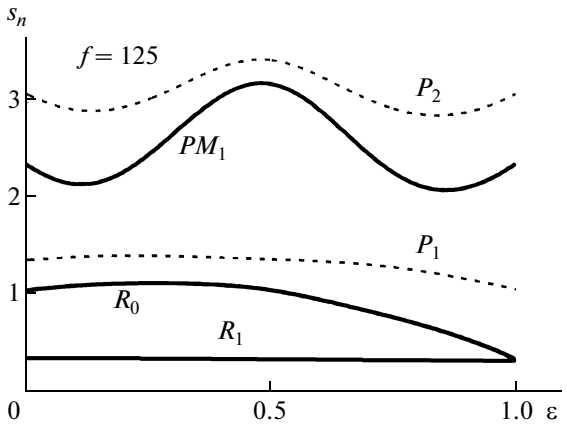

Fig. 5. Influence of porosity $\varepsilon_1 = \varepsilon_2 = \varepsilon$ on the slowness s_n of the pore and Rayleigh modes (see also Figs. 3a and 3b for $f = 125$ Hz).

obtained upon averaging the parameters of the water-saturated half-space (R_s, dash–dotted line), it is the principal Rayleigh wave, while R_1 is the additional mode occurring due to the medium porosity.

The occurrence of such additional waves (i.e., additional poles ζ_n) is well illustrated by the plots of dispersion curves $s_n(f)$ (f is the frequency in Hz) for the three-layered half-space (Fig. 3). Two upper layers with the thickness $h_1 = h_2 = 0.5$ m with the parameters (22), (23) can be water-saturated ($\varepsilon = 0.1$) or purely elastic ($\varepsilon = 0$) and the lower half-space in all examples is elastic with the parameters $\lambda = 59.06$, $\mu = 26.12$ GPa, and $\rho = 2700$ kg/m^3. The series of four sets of dispersion curves for all possible combinations of the porosity ε_k of two upper layers is presented:

(a) $\varepsilon_1 = \varepsilon_2 = 0$ is the purely elastic medium (actually, the two-layered half-space with a 1-m-thick upper layer and properties of elastic skeleton (23));

(b) $\varepsilon_1 = \varepsilon_2 = 0.1$ is the two-layered half-space and the upper layer is fluid-saturated with open pores;

(c) $\varepsilon_1 = 0.1$, $\varepsilon_2 = 0$ is the three-layered half-space with the porous upper layer with a thickness of 0.5 m;

(d) $\varepsilon_1 = 0$, $\varepsilon_2 = 0.1$ is the three-layered half-space with the porous internal layer.

The comparison of these cases shows that the presence of porosity practically does not change the characteristics (slowness) of Rayleigh-type waves for the elastic two-layered half-space shown in Fig. 3a (similarly to the slight difference of the wave R_2 in Fig. 2b and the classical Rayleigh wave), but in this case additional modes PM_n (pore modes) occur. Output points of the dispersion curves of these modes (cutoff frequencies) are inversely proportional to the thickness of the porous layer and, therefore, are shifted to the right with decreasing thickness (compare Figs. 3b and 3c).

In the case of the upper elastic layer (Fig. 3d), practically dispersionless pore mode PM_0 occurs and the cutoff frequency of the following mode PM_1 tends to the right beyond the frequency range shown in Fig. 3. The mode PM_0 is present for any thickness of the upper layer h_1 up to its degeneration at $h_1 \to 0$ into an infinitely thin film closing pores (see Fig. 4a for $\varepsilon_1 = \varepsilon_2 = 0.1$ but with boundary condition (11) for closed pores). The amplitude of this additional mode can be essentially higher than the amplitude of principal Rayleigh modes R_n. This fact is illustrated in Fig. 4b; this figure shows the dependences of the absolute value of the amplitude factors $\mathbf{a}_n$ included in wave representation (3) on the thickness of the upper layer h_1 for

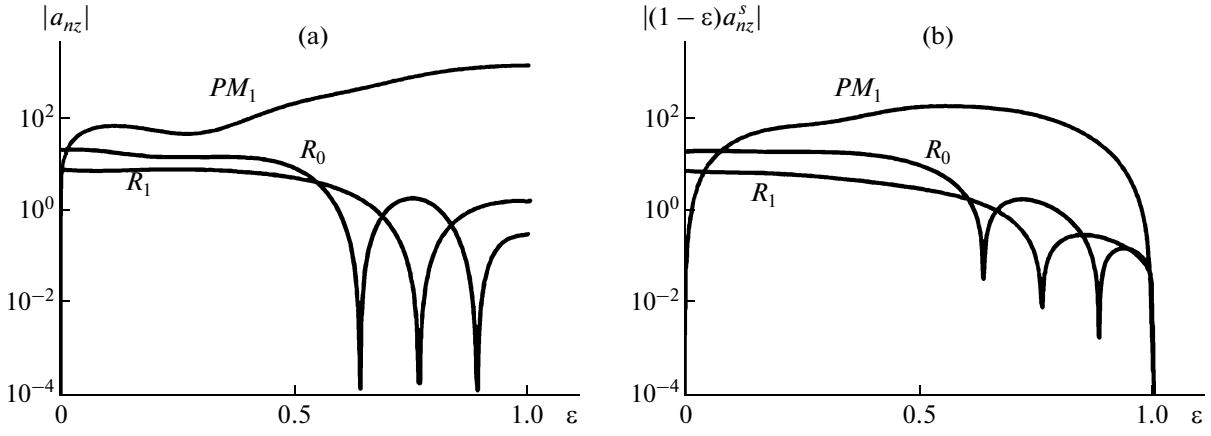

Fig. 6. (a) Amplitude of normal components a_z of surface waves excited in the two-layered half-space by the normal concentrated load depending on the porosity ε of the surface layer and (b) contribution to the amplitude of displacements of elastic skeleton (in the logarithmic scale).

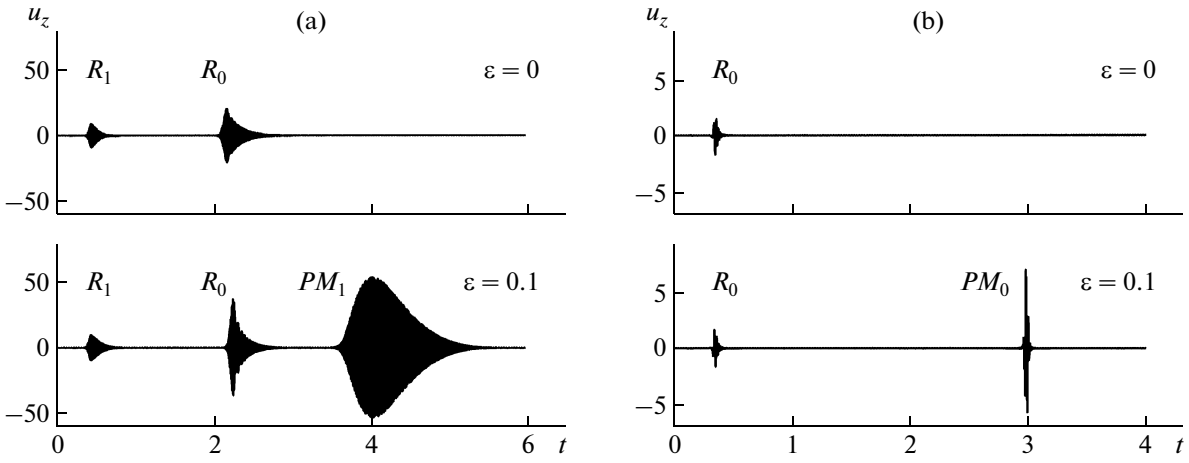

Fig. 7. Illustration of occurrence of additional signals in the presence of porosity ($\varepsilon = 0.1$) on theoretical seismograms for the waveguide with (a) open ($f_c = 125$ Hz) and (b) closed ($f_c = 40$ Hz) pores.

$h = h_1 + h_2 = 1$, $\varepsilon_1 = 0$, $\varepsilon_2 = 0.1$, $f = 40$ Hz. For $h_1 = 0$ this corresponds to the case of the upper porous layer with closed pores (see Fig. 4a), for $h_1 = 0.5$ m the medium is the same as in Fig. 3d, and for $h_1 = 1$ m, it is the same as in Fig. 3a. In the latter case the mode PM_0 is absent, since the corresponding residual included in the representation of $\mathbf{a}_n$ for $h_1 = 1$ vanishes and the pole becomes removable.

Note that while dispersion curves can be obtained in the framework of the modal analysis, amplitude characteristics shown in Fig. 4b and below depend not only on the medium properties but also on the source type. The concentrated vertical load $\mathbf{q} = p_0\delta(x, y)\mathbf{i}_3 e^{-i\omega t}$ is taken as the source for certainty; i.e., actually the amplitude of elements of the third column of the matrix K is considered.

Figures 5 and 6 show the dependence of the slowness s_n on ε and the amplitude of corresponding Rayleigh modes for the two-layered space ($\varepsilon_1 = \varepsilon_2 = \varepsilon$) at the fixed frequency $f = 125$ Hz (for $\varepsilon = 0.1$ the parameters of the medium are the same as in Fig. 3b). For chosen dependence (22) of the upper layer properties, the slowness of Biot body wave changes with increasing ε in a wavy way (Fig. 5, dashed line P_2). The slowness of the additional pore mode PM_1 behaves in a similar way. The slowness of the principal Rayleigh wave R_0 also depends on porosity, decreasing with increasing ε similar to the case of the homogeneous half-space (Fig. 2a), and the velocity of the next principal mode R_1 is practically independent of ε. In the limit for $\varepsilon = 1$ the characteristics of all presented modes coincide with the corresponding characteristics of Scholte–Stoneley waves for the layer of acoustic fluid on the elastic half-space.

The plots in Fig. 6a show the dependence of ε on the amplitude of vertical components a_{nz} of the displacement vectors of these modes ($f = 125$ Hz, $z = 0$) and the fraction $(1 - \varepsilon)a_{nz}^s$ related to the elastic skeleton (Fig. 6b). Due to a large value spread, the amplitude characteristics are shown in the logarithmic scale. Although in the elastic medium the pore mode is absent ($|\mathbf{a}_n| = 0$ for PM_1 and $\varepsilon = 0$), its amplitude becomes larger than the amplitude of the waves R_0 and R_1 already for rather small values of ε both for vertical displacements on the whole and displacements of the elastic phase. It is also interesting to note that there exist porosity values ($\varepsilon \approx 0.63$ and 0.87 for R_0 and $\varepsilon \approx 0.78$ for R_1) for which the indicated principal modes are practically not excited.

The dominating character of the additional pore mode is manifested in theoretical seismograms constructed for the vertical component of displacements of the surface $u_z(t)$ at the distance $r = 1$ km from the nonstationary source $\mathbf{q} = p(t)\delta(x, y)\mathbf{i}_3$ (Fig. 7). The form of the initial pulse $p(t)$ is determined by the Hanning frequency spectrum with the central frequency f_c and the range half-width Δf,

$$P(\omega) = \begin{cases} p_0 \cos^2 \dfrac{\pi(f - f_c)}{2\Delta f}, & |f - f_c| < \Delta f, \\ 0, & |f - f_c| > \Delta f, \omega = 2\pi f. \end{cases}$$

The occurrence of the additional signal transferred by the pore mode can be seen in the case of comparison with the seismograms for the two-layered elastic half-space ($\varepsilon = 0$, dispersion properties see Fig. 3a) in the upper parts of Figs. 7a and 7b. The lower parts of these figures show the seismograms for the two-layered half-space with the upper porous layer with the thickness $h = h_1 + h_2 = 1$ m (Fig. 7a) and the three-layered

half-space with the internal porous layer $h_2 = 0.5$ (Fig. 7b). The dispersion properties of these layers are shown in Figs. 3b and 3d, respectively.

In the first case, the pulse $p(t)$ with the characteristics $f_c = 125$, $\Delta f = 25$ Hz excites three modes R_1, R_0, and PM_1 with the group velocities of the wave packets $c_n = d\omega/d\xi$ equal to 2.2, 0.43, and 0.25 km/s, respectively. The arrival times for signals transferred by these modes, $t_{R_1} = 0.45$, $t_{R_0} = 2.34$, and $t_{PM} = 4.03$ s agree well with the principal maxima in the lower seismogram (Fig. 7a).

The second example (Fig. 7b) demonstrates the occurrence of additional wave packet with large amplitude which arrives at the observation point with the group velocity $c_{PM} = 1/3$ km/s. Here, the signal with the low central frequency $f_c = 40$ Hz and the half-width $\Delta f = 40$ Hz at which there are no additional pore modes in the first case (Fig. 3b), is taken, i.e., the form of $u_z(t)$ for $\varepsilon = 0.1$ is practically the same as for $\varepsilon = 0$.

Obviously, the ratio of amplitudes of excited modes depends on the combination of elastic properties of the layers D_k. The results presented above were obtained for the case of relatively hard lower half-space D_N ($\mu_N/\mu = 85$, where μ_N is the shear modulus of the elastic material of D_N and μ is that of the porous layers). If the plots of the amplitude of excited modes as a function of μ_N/μ are considered, for example, for the second case (not show here), the amplitude of R_0 is higher than that of PM_0 in the range $1.3 < \mu_N/\mu < 5$. For $\mu_N/\mu > 2$ the value of the latter is practically unchanged, while the amplitude of R_0 monotonically decreases, and for $\mu_N/\mu = 85$ it becomes such as shown in Fig. 4b for $h_1 = 0.5$.

ACKNOWLEDGMENTS

We thank S.A. Voitsekhovskaya, who attracted our attention to wave problems for porous media.

This work was supported by the Russian Ministry of Education and Science, project no. 2.1.1/1231.

REFERENCES

1. Ya. I. Frenkel', Izv. Akad. Nauk SSSR, Geol. Geofiz. **8**, 133 (1944).
2. M. A. Biot, J. Acoust. Soc. Am. **28**, 168 (1956).
3. T. J. Plona, Appl. Phys. Lett. **36**, 259 (1980).
4. O. Kelder and D. M. J. Smeulders, Geophys. **62**, 1794 (1997).
5. L. A. Molotkov, *Investigation of Wave Propagation in Porous and Fractured Media on the Basis of Effective Models of Biot and Layered Media* (Nauka, St.-Petersbourg, 2001) [in Russian].
6. S. Feng and D. L. Johnson, J. Acoust. Soc. Am. **74**, 906 (1983).
7. A. A. Gubaidullin and O. Yu. Boldyreva, Akust. Zh. **52**, 201 (2006) [Acoust. Phys. **52**, 163 (2006)].
8. N. S. Gorodetskaya, Akust. Visn. **10** (2), 43 (2007).
9. N. S. Gorodetskaya and T. V. Sobol', Akust. Visn. **11** (1), 3 (2008).
10. N. S. Gorodetskaya, T. V. Sobol', and L. P. Zubareva, Akust. Visn. **11** (3), 50 (2008).
11. M. J. Mayer, P. B. Nagy, L. Adler, B. P. Bonner, and R. Streit, J. Acoust. Soc. Am. **79**, 249 (1986).
12. A. N. Norris, Geophysics **54**, 330 (1989).
13. I. I. Vorovich and V. A. Babeshko, *Mixed Dynamic Problems of Elasticity Theory in Unbounded Domains* (Nauka, Moscow, 1979) [in Russian].
14. E. V. Glushkov, N. V. Glushkova, and M. V. Golub, Akust. Zh. **52**, 314 (2006) [Acoust. Phys. **52**, 259 (2006)].
15. E. Glushkov and N. Glushkova, J. Comput. Acoust. **9**, 889 (2001).
16. V. A. Babeshko, E. V. Glushkov, and N. V. Glushkova, Zh. Vych. Mat. Mat. Fiz. **27**, 93 (1987).
17. E. V. Glushkov, N. V. Glushkova, A. A. Eremin, and V. V. Mikhas'kiv, Prikl. Mat. Mekh. **73**, 622 (2009).
18. E. V. Glushkov, N. V. Glushkova, and A. S. Krivonos, Prikl. Mat. Mekh. **74** (3), 419 (2010).
19. L. A. Molotkov, Zap. Nauch. Seminarov POMI **264**, 217 (2000).
20. R. Burridge and C. A. Vargas, Geophys. J. Roy. Astr. Soc. **58**, 61 (1979).
21. G. Bonnet, J. Acoust. Soc. Am. **82**, 1758 (1987).
22. Yu. M. Zaslavsky, Akust. Zh. **51**, 759 (2005) [Acoust. Phys. **51**, 653 (2005)].
23. E. V. Glushkov, N. V. Glushkova, and S. I. Fomenko, in *Actual Aspects of Physico-Mechanical Studies. Acoustics and Waves* (Naukova Dumka, Kiev, 2007), pp. 73–82 [in Russian].
24. S. I. Fomenko, Candidate's Dissertation in Physico-Mathematical Sciences (Kubansk. Gos. Univ., 2008).
25. V. M. Seimov, A. N. Trofimchuk, and O. A. Savitskii, *Oscillations and Waves in Layered Media* (Naukova Dumka, Kiev, 1990) [in Russian].